Articles

Evaluation of Phosphorescent Rhenium and Iridium Complexes in Polythionylphosphazene Films for Oxygen Sensor Applications

Loan Huynh, Zhuo Wang, Jian Yang, Valentina Stoeva, Alan Lough, Ian Manners,* and Mitchell A. Winnik*

Department of Chemistry, University of Toronto, 80 St. George Street, Toronto, Ontario M5S 3H6, Canada

Received December 17, 2004. Revised Manuscript Received June 1, 2005

Three metal complexes—[Re(bpy)(CO)$_3$(CN-*t*-Bu)]Cl (**1**) (where bpy = 2,2-bipyridine), Bu$_4$N[Ir(ppy)$_2$(CN)$_2$] (**2**), and Ir(ppy)$_3$ (**3**) (where ppy = 2-phenylpyridine and Bu$_4$N = tetrabutylammonium cation)—were evaluated as oxygen sensors in poly((*n*-butylamino)thionylphosphazene) (*n*BuPTP) matrixes. The phosphorescent dyes **2** and **3** exhibit long lifetimes and high quantum yields in degassed dichloromethane and toluene solutions and when dissolved in the polymer matrix. These two dyes exhibited exponential decays both in solution and in the polymer films, with somewhat longer lifetimes (for **2**, $\tau_0 = 4.78$ μs; for **3**, $\tau_0 = 1.40$ μs) in the polymer film. All three dyes gave linear Stern−Volmer plots, but **1** was rather sensitive to photodecomposition. The slopes of the Stern−Volmer plots for these dyes were compared to those measured previously for platinum octaethyl porphine (PtOEP) and ruthenium tris-diphenylphenanthroline chloride ([Ru(dpp)$_3$]Cl$_2$. Attempts to explain the differences in slope using τ_0 as the sole scaling parameter were unsuccessful. To explain these results, we calculated the effective capture radius for quenching by oxygen, which was 1.7 nm for **2** and 2.7 nm for **3**, relative to a value of 1.0 nm for PtOEP. Thus, dye **3** is 2.7 times more sensitive to quenching by oxygen than PtOEP and more than 5 times more sensitive than [Ru(dpp)$_3$]Cl$_2$.

1. Introduction

Phosphorescent materials, which contain luminophores that can be quenched by oxygen, are of interest in the fabrication of oxygen-sensing devices for biomedical and barometric applications, as well as environmental monitoring.[1−8] The photophysical and photochemical properties of phosphorescent transition-metal complexes such as Ru(II), Os(II), Re(I), Rh(III), and Ir(III) species have been thoroughly investigated over the past two decades.[1,9−14] The metals in many of these complexes possess an octahedral d^6 electron configuration, which is often adaptable for luminescent sensor design because of the presence of high extinction coefficients, as a result of metal-to-ligand charge transfer.[1,9,10,15−17] These complexes display molecular phosphorescence because of strong spin-orbit coupling associated with the metal. Various oxygen-sensing materials have been developed in which a luminescent dye is dissolved or otherwise immobilized in a polymer matrix,[9,10,15−17] and several have been applied in wind tunnel research as pressure-sensitive paints (PSPs).[2] Recently, we have developed sensors in which a Ru(phen)$_3$Cl$_2$ complex derivative (where phen = 1,10-phenanthroline) has been successfully introduced into poly((*n*-butylamino)thionylphosphazene) (*n*BuPTP) films either by dissolution and through covalent attachment to the polymer backbone.[9,10] The ruthenium dye covalently bonded to

* To whom correspondence should be addressed. E-mail: imanners@chem.utoronto.ca; mwinnik@chem.utoronto.ca.

(1) King, K. A.; Spellane, P. J.; Watts, R. J. *J. Am. Chem. Soc.* **1985**, *107*, 1431.
(2) Gouterman, M. *J. Chem. Educ.* **1997**, *74*, 697.
(3) Carraway, E. R.; Demas, J. N.; DeGraff, B. A.; Bacon, J. R. *Anal. Chem.* **1991**, *63*, 337.
(4) Moreno-Bondi, M. C.; Wolfbeis, O. S.; Leiner, M. J. P.; Schaffar, B. P. H. *Anal. Chem.* **1990**, *62*, 2377.
(5) Preininger, C.; Klimant, I.; Wolfbeis, O. S. *Anal. Chem.* **1994**, *66*, 1841.
(6) Bacon, J. R.; Demas, J. N. *Anal. Chem.* **1987**, *59*, 2780.
(7) Demas, J. N.; DeGraff, B. A. *Anal. Chem.* **1991**, *63*, 829A.
(8) Marco, G. D.; Lanza, M.; Campagna, S. *Adv. Mater.* **1995**, *7*, 468.
(9) Pang, Z.; Gu, X.; Yekta, A.; Masoumi, Z.; Coll, J. B.; Winnik, M. A.; Manners, I. *Adv. Mater.* **1996**, *8*, 768.
(10) Wang, Z.; McWilliams, A. R.; Evans, C. E. B.; Lu, X.; Chung, S.; Winnik, M. A.; Manners, I. *Adv. Funct. Mater.* **2002**, *12*, 415.
(11) Lamansky, S.; Djurovich, P.; Murphy, D.; Abdel-Razzaq, F.; Kwong, R.; Tsyba, I.; Bortz, M.; Mui, B.; Bau, R.; Thompson, M. E. *Inorg. Chem.* **2001**, *40*, 1704.
(12) Tamayo, A. B.; Alleyne, B. D.; Djurovich, P. I.; Lamansky, S.; Tsyba, I.; Ho, N. N.; Bau, R.; Thompson, M. E. *J. Am. Chem. Soc.* **2003**, *125*, 7377.
(13) Lamansky, S.; Djurovich, P.; Murphy, D.; Abdel-Razzaq, F.; Lee, H.-E.; Adachi, C.; Burrows, P. E.; Forrest, S. R.; Thompson, M. E. *J. Am. Chem. Soc.* **2001**, *123*, 4304.
(14) Rossenaar, B. D.; Stufkens, D. J.; Vlcek, A., Jr. *Inorg. Chem.* **1996**, *35*, 2902.
(15) Demas, J. N.; DeGraff, B. A.; Coleman, P. B. *Anal. Chem.* **1999**, 71, 793A.
(16) Lakowicz, J. R. *Principles of Fluorescence Spectroscopy*, 2nd Edition; Kluwer Acadamic/Plenum: New York, 1999.
(17) Demas, J. N.; DeGraff, B. A.; Coleman, P. B. *Coord. Chem. Rev.* **2001**, *211*, 317.

10.1021/cm047794r CCC: $30.25
Published on Web 08/20/2005

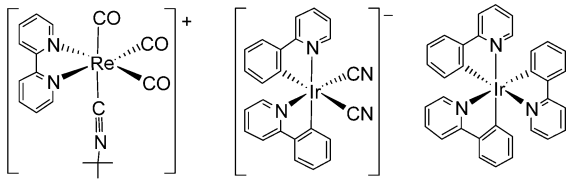

Figure 1. Transition-metal complexes studied in this paper.

*n*BuPTP exhibited linear Stern−Volmer (SV) behavior, and its sensitivity to oxygen quenching was significantly improved, in comparison to the case where the dye was simply dissolved in the polymer film.

In another study where cyclometalated Ir complexes such as $Bu_4N[Ir(ppy)_2(CN)_2]$, $Bu_4N[Ir(ppy)_2(NCO)_2]$, and $[Ir(ppy)_2(acac)]$ (where ppy = 2-phenylpyridine, acac = acetoylacetonate, and Bu_4N = tetrabutylammonium cation) were used as phosphorescent emitters in organic light-emitting device (OLED) applications,[13,18,19] the excited states generated during the electroluminescence exhibited lifetimes in the microsecond range.[20] In contrast, the phosphorescence lifetimes of other metal complexes such as rhodium are typically in the nanosecond regime and give measurable emission only at low temperatures.[20]

Our previous studies of PtOEP (where OEP = octaethylporphyrin), PtTFPP (where TFPP = tetrakis(pentafluorophenyl)porphyrin), PtOEPK (where OEPK = octaethylporphyrin ketone), $[Ru(dpp)_3]Cl_2$ (where dpp = 4,7-diphenylphen), and $Ru(phen)_3Cl_2$ complexes indicated that these complexes form promising oxygen sensors when immobilized in *n*BuPTP matrixes.[9,10,21] However, higher quantum yields have been reported for other complexes, which would be an advantage for the optimization of the sensors. For example, for PSP applications, it is important that the luminescent dyes have high quantum yield for emission, with a lifetime of few microseconds or less. In this paper, we report the evaluation of the oxygen-sensing properties of the metal complexes $[Re(bpy)(CO)_3(CN\text{-}t\text{-}Bu)]Cl$,[22,23] $Bu_4N[Ir(ppy)_2(CN)_2]$, and $Ir(ppy)_3$[12] (Figure 1) immobilized in *n*BuPTP.[9,10]

Rhenium and iridium complexes are of interest, because of the strong spin−orbit coupling associated with third-row transition elements, which enables efficient access to long-lived strongly emitting phosphorescent excited states.[11] The luminescence of many Re(I) complexes is also characterized by high quantum yields ($\Phi = 0.4-0.7$) and long lifetimes at room temperature, with τ values of 1−100 μs.[17,24] With these promising properties, Re(I) complexes become attractive for applications as sensors and molecular probes.[17] For example, the complex $[Re(CO)_3(bpy)(CN\text{-}t\text{-}Bu)]^+$ is reported to have a lifetime of $\tau_0 = 2.0$ μs with a quantum yield of $\Phi = 0.6$ in deoxygenated CH_2Cl_2 solution.[24]

Many recent studies on the iridium pseudo-halogen and cyclometalated complexes have demonstrated that iridium complexes have relatively long excited-state lifetimes and show intense phosphorescence at room temperature.[12,13,25−29] For example, $Ir(ppy)_3$ has a lifetime of $\tau_0 = 2.0$ μs with a quantum yield of $\Phi = 0.5$ in toluene,[30] and the $Bu_4N[Ir(ppy)_2(CN)_2]$ complex has a lifetime of $\tau_0 = 3.1$ μs with a quantum yield of $\Phi = 0.94$[18] in dichloromethane, whereas the lifetime of an analogous transition-metal complex (such as $[Ru(bpy)_3]Cl_2$ (where bpy = 2,2′-bipyridine)) is $\tau_0 = 0.6$ μs with a quantum yield of only $\Phi = 0.042$.[31]

For our studies, we chose the rhenium and iridium complexes **1**−**3** for sensor design as the photoluminescent (PL) excited states of these phosphorescent metal complexes, which have long lifetimes and high quantum yields. We chose, as our matrix, the polymer *n*BuPTP, because of its useful mechanical properties and good oxygen permeability.[9,10,23,27,32−34] In addition, the properties of this polymer can be modified by variation of the side-group substituents.

2. Results and Discussion

2.1. Synthesis and Characterization of Complexes 1−3. The synthesis of the rhenium dye was accomplished using a modified literature procedure[22] (Scheme 1). Ligand exchange of $Re(bpy)(CO)_3Cl$ with $Ag[OSO_2CF_3]$ gave a rhenium(I) triflate species. Reaction of the triflate species with $NaBAr'_4$ ($Ar' = C_6H_3(CF_3)_2$),[35] followed by the addition of CN-*t*-Bu to the reaction mixture, yielded a crude product that was recrystallized to give a pure $[Re(CO)_3(bpy)(CN\text{-}t\text{-}Bu)]BAr'_4$ as a yellow crystalline solid. The IR bands in CH_2Cl_2 solution were observed at 2044, 1970, and 1943 cm^{-1} in the CO stretching region. The ^1H NMR and ^{13}C NMR spectra were in accordance with the assigned structure, which was further confirmed by a single-crystal X-ray diffraction (XRD) study (see Figure 2 and Table 1). Counteranion exchange to give the chloride salt was performed using $[Bu_4N]Cl$.

The iridium pseudo-halogen and cyclometalated complexes **2** and **3** were also synthesized using procedures reported in the literature.[12,18,20] The ^1H and ^{13}C NMR data of these complexes were in accord with those previously reported and were consistent with the heterocyclic rings of the C, N ligands being present in a trans arrangement.[12,18,20]

(18) Nazeeruddin, Md. K.; Humphry-Baker, R.; Berner, D.; Rivier, S.; Zuppiroli, L.; Graetzel, M. *J. Am. Chem. Soc.* **2003**, *125*, 8790.
(19) Lamansky, S.; Djurovich, P. I.; Abdel-Razzaq, F.; Garon, S.; Murphy, D. L.; Thompson, M. E. *J. Appl. Phys.* **2002**, *92*, 1570.
(20) Sprouse, S.; King, K. A.; Spellane, P. J.; Watts, R. J. *J. Am. Chem. Soc.* **1984**, *106*, 6647.
(21) Lu, X.; Han, B.-H.; Winnik, M. A. *J. Phys. Chem. B* **2003**, *107*, 13349.
(22) Hevia, E.; Perez, J.; Riera, V.; Miguel, D.; Kassel, S.; Rheingold, A. *Inorg. Chem.* **2002**, *41*, 4673.
(23) Ruffolo, R.; Evans, C. E. B.; Liu, X.-H.; Ni, Y.; Pang, Z.; Park, P.; McWilliams, A. R.; Gu, X.; Lu, X.; Yekta, A.; Winnik, M. A.; Manners, I. *Anal. Chem.* **2000**, *72*, 1894.
(24) Sacksteder, L.; Lee, M.; Demas, J. N.; DeGraff, B. A. *J. Am. Chem. Soc.* **1993**, *115*, 8230.
(25) Donckt, V. E.; Camerman, B.; Hendrick, F.; Herne, R.; Vandeloise, R. *Bull. Soc. Chim. Belg.* **1994**, *103*, 207.
(26) Leslie, W.; Batsanov, A. S.; Howard, J. A. K.; Williams, J. A. G. *J. Chem. Soc.*; Dalton Trans.: **2004**, 623.
(27) Licini, M.; Williams, J. A. G. *Chem. Commun.* **1999**, 1943.
(28) DeRosa, M. C.; Hodgson, D. J.; Enright, G. D.; Dawson, B.; Evans, C. E. B.; Crutchley, R. J. *J. Am. Chem. Soc.* **2004**, *126*, 7619.
(29) DeRosa, M. C.; Mosher, P. J.; Yap, G. P. A.; Focsaneanu, K.-S.; Crutchley, R. J.; Evans, C. E. B. *Inorg. Chem.* **2003**, *42*, 4864.
(30) Wang, Y.; Herron, N.; Grushin, V. V.; LeCloux, D.; Petrov, V. *Appl. Phys. Lett.* **2001**, *79*, 449.
(31) Houten, J. V.; Watts, R. J. *J. Am. Chem. Soc.* **1975**, *97*, 3843.
(32) Liang, M.; Manners, I. *J. Am. Chem. Soc.* **1991**, *113*, 4044.
(33) Ni, Y.; Park, P.; Liang, M.; Massey, M.; Waddling, C.; Manners, I. *Macromolecules* **1996**, *29*, 3401.
(34) Gates, D. P.; Manners, I. *J. Chem. Soc., Dalton Trans.* **1997**, 2525.
(35) Brookhart, M.; Grant, B.; Volpe, A. F., Jr. *Organometallics* **1992**, *11*, 3920.

Scheme 1. Synthesis of 1

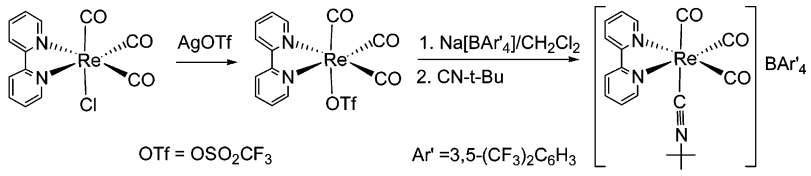

(**1**)

Table 1. Selected Bond Lengths and Bond Angles for Complex 1[a]

Bond Length Data		Bond Angle Data	
bond	length (Å)	bond angle	measurement (deg)
Re_1-C_1	1.945(9)	$C_3-Re_1-C_2$	88.8(3)
Re_1-C_2	1.924(9)	$C_3-Re_1-C_1$	88.4(4)
Re_1-C_3	1.916(9)	$C_1-Re_1-C_4$	177.0(3)
Re_1-C_4	2.092(8)	$C_2-Re_1-C_4$	90.1(3)
Re_1-N_2	2.174(5)	$C_2-Re_1-N_2$	99.4(3)
Re_1-N_3	2.174(5)	$C_4-Re_1-N_2$	87.9(2)
N_1-C_4	1.142(9)	$C_1-Re_1-N_3$	91.9(3)
N_1-C_5	1.466(9)	$C_2-Re_1-N_3$	174.1(3)
O_1-C_1	1.162(10)	$C_1-Re_1-N_2$	95.2(3)
O_2-C_2	1.145(10)	$N_3-Re_1-N_2$	74.8(2)
O_3-C_3	1.170(10)	$C_4-Re_1-N_3$	89.1(2)

[a] Estimated standard deviations given in parentheses.

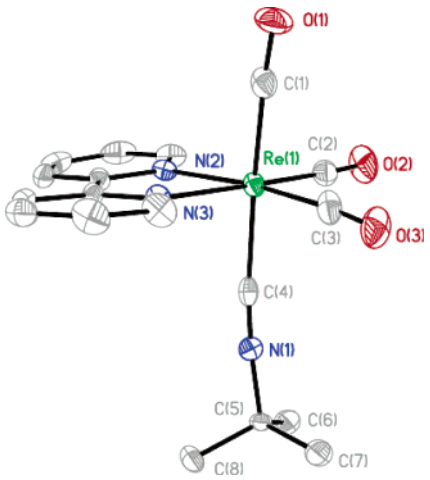

Figure 2. X-ray structure of $[Re(CO)_3(bpy)(CN\text{-}t\text{-}Bu)]BAr'_4$ (**1**). The counteranion is not shown.

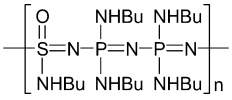

Figure 3. Schematic depiction of the poly((*n*-butylamino)thionylphosphazene).

The synthesis of *n*BuPTP (Figure 3) was achieved through the thermal ring opening polymerization of the cyclic thionylphosphazene $[NSOCl(NPCl_2)_2]$.[32,33] The resulting polymer $[NSOCl(NPCl_2)_2]_n$ was then treated with an excess amount of *n*-butylamine to produce *n*BuPTP as a hydrolytically stable amorphous elastomer with a glass transition temperature of $T_g = -16$ °C.[33] The oxygen permeability of *n*BuPTP has been reported to be ca. 1.8×10^{-12} mol cm^{-1} s^{-1} atm^{-1}.[23,36]

2.2. Photophysical Properties of Complexes 1−3. The UV−vis absorption and emission spectra of complexes **1**, **2**, and **3**, which have been obtained from degassed solutions, are consistent with those reported in the literature[12,18,20] (Figure 4). The emission maximum for the rhenium complex in CH_2Cl_2 solution is located at $\lambda_{max} = 507$ nm, whereas those for the iridium complexes **2** (in CH_2Cl_2) and **3** (in toluene) are $\lambda_{max} = 470$ nm and $\lambda_{max} = 510$ nm, respectively. Lifetime measurements of these complexes show that all of the dyes have values in the range of $\tau_0 = 1.0-3.2$ μs in degassed solution, which are in accordance with those reported in the literature.[12,18,24]

We also investigated the photostability of the dyes in *n*BuPTP films and in degassed solutions. Film samples **1A**, **2A**, and **3A**, containing dyes **1**−**3**, respectively, at 500 ppm, were prepared and exposed to bright sunlight. After 5 h of exposure, the film samples exposed to air showed serious photoinduced deterioration. The samples **1A** and **3A** no longer showed any PL, whereas the PL of sample **2A** was very weak. After 5 h of exposure to the sunlight, the infrared (IR) spectra showed the disappearance of the CN stretch at 2250 cm^{-1} for sample **2A** ($Bu_4N[Ir(ppy)_2(CN)_2]$) and the disappearance of υ_{CO} at 2044, 1970, and 1943 cm^{-1} for sample **1A** ($[Re(bpy)(CO)_3(CN\text{-}t\text{-}Bu)]Cl$). However, the emission spectra of **2** in CH_2Cl_2 (1×10^{-5} M) and of **3** in toluene (1×10^{-5} M) show that degassed solutions of complexes **2** and **3** are photostable after 5 h of exposure to bright sunlight. The lowest photostability was detected for rhenium complex **1** is accordance with the well-documented photolability of metal carbonyls.[37]

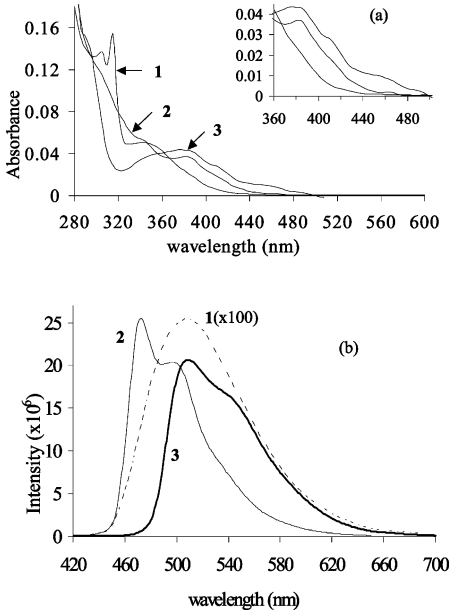

Figure 4. (a) Absorption spectra and (b) emission spectra at 25 °C in degassed solution of **1** (in CH_2Cl_2, 1×10^{-5} M, $\lambda_{exc} = 340$ nm), **2** (in CH_2Cl_2, 1×10^{-5} M, $\lambda_{exc} = 340$ nm) and **3** (in toluene, 1×10^{-5} M, $\lambda_{exc} = 379$ nm).

(36) Masoumi, Z.; Stoeva, V.; Yekta, A.; Pang, Z.; Manners, I.; Winnik, M. A. *Chem. Phys. Lett.* **1996**, *261*, 551.

2.3. Photoluminescence Quenching Concepts. For dyes in fluid solution in the presence of a quencher Q, the reduction in PL intensity (I) and the decrease in the excited-state lifetime τ normally follows the Stern−Volmer (SV) equation:[15]

$$\frac{I_0}{I} = \frac{\tau_0}{\tau} = 1 + k_q \tau_0 [Q] \quad (1)$$

In this expression, [Q] is the molar concentration of quencher, k_q is the second-order quenching rate constant, and the subscript zero ("0") refers to the values in the absence of quencher. When the quencher is introduced into the system as a gas such as oxygen, one commonly measures the intensity and the excited-state lifetime as a function of external partial pressure (e.g., p_{O_2}), and eq 1 can be rewritten in terms of the Henry's Law constant S_{O_2}, which relates external pressure to solute concentration:

$$\frac{I_0}{I} = \frac{\tau_0}{\tau} = 1 + k_q \tau_0 S_{O_2} p_{O_2} \quad (2)$$

For oxygen sensors that are based on polymer films, it is often convenient to express the SV equation in a more phenomenological form:

$$\frac{I_0}{I} = \frac{\tau_0}{\tau} = 1 + K_{SV} p_{O_2} \quad (3)$$

where the Stern−Volmer constant K_{SV} contains all of the constants that relate oxygen partial pressure (p_{O_2}) to the changes in intensity and lifetime. For an ideal sensor, where the dyes exist in a single uniform quenching environment, linear SV behavior is expected. However, deviations have been observed, and these are often attributed to sample heterogeneities in which the dyes are distributed in different types of oxygen quenching sites in the matrix. A change in either intensity or decay time can be used to quantify the amount of oxygen present. A useful test of a well-behaved system is whether the intensity ratios and lifetime ratios yield the same response to a change in pressure. Values of K_{SV} vary from dye to dye, and higher values of K_{SV} indicate that the dye is more sensitive to oxygen quenching;[16,17,24] however, as indicated in eqs 1 and 2, this enhanced sensitivity is normally associated with dyes with long excited-state lifetimes. This is the reason many PL oxygen sensors are based on phosphorescent dyes.

It is possible to perform a deeper analysis of the PL quenching experiments. Oxygen quenching is normally diffusion-controlled. Thus, one can equate k_q with the second-order diffusion-controlled rate constant k_{diff}. In terms of the theory of partially diffusion controlled reactions, k_{diff} is related to the diffusion constant D_{O_2} of oxygen in the medium by the expression

$$k_{diff} = 4\pi N_A \alpha R_{eff} D_{O_2} \quad (4)$$

Here, N_A is Avogadro's number, R_{eff} is the capture radius at which quenching occurs, and α is the quenching efficiency per encounter.[16,21,38,39]

The introduction of eq 4 into eq 2 leads to

$$\frac{I_0}{I} = \frac{\tau_0}{\tau} = 1 + 4\pi N_A \tau_0 \alpha R_{eff} D_{O_2} S_{O_2} p_{O_2} \quad (5)$$

Because the permeability of a gas in a medium is defined as the product of its diffusion constant times its solubility coefficient ($P_{O_2} = D_{O_2} \times S_{O_2}$),[16] eq 4 can be rewritten, in terms of intensities, as

$$\frac{1}{\tau_0}\left(\frac{I_0}{I} - 1\right) = 4\pi N_A \alpha R_{eff} P_{O_2} p_{O_2} \quad (6)$$

and, in terms of lifetimes, as

$$\frac{1}{\tau_0} = \frac{1}{\tau} + 4\pi N_A \alpha R_{eff} P_{O_2} p_{O_2} \quad (7)$$

For PL quenching experiments in a polymer matrix, eqs 6 and 7 can be used to obtain a value for P_{O_2} if linear SV plots are obtained and a reasonable assumption can be made about the magnitude of αR_{eff} in the system. For example, we have made the assumption that $\alpha R_{eff} = 1.0$ nm for oxygen quenching of PtOEP in *n*BuPTP, and we used this value to calculate a value of $P_{O_2} = 4.0 \times 10^{-12}$ mol s^{-1} cm^{-1} atm^{-1} for this polymer at 23 °C.[21] Alternatively, if PL quenching experiments can be performed in a polymer for which the oxygen permeability is known independently, then a value of αR_{eff} can be determined from analysis of the SV plots, in terms of eqs 5 and 6. We know of no polymer in which both measurements have been made on the same system. Determination of P_{O_2} by traditional measurements of gas transport across a membrane requires free-standing films of uniform thickness. For low-T_g polymers such as poly(dimethylsiloxane) (PDMS), these measurements must be made on cross-linked films in which one assumes that cross-linking has little effect on gas permeability.

Although one may think of α and R_{eff} as constants characteristic of a chromophore and a quenching mechanism, in reality, because of multiple collisions, the magnitude of αR_{eff} varies with factors such as temperature that affect the diffusion rates in the system. In the limit of $D_{O_2} \rightarrow 0$, α approaches a value of unity and R_{eff} approaches the true capture radius for the quenching process.

An issue of greater concern for us is whether different dyes exhibit different intrinsic sensitivities to quenching by oxygen. This is important knowledge for sensor design. Different dyes in a common polymer matrix normally exhibit different SV slopes. If these differences occur only as a consequence of the different unquenched lifetimes of the dyes, then the oxygen-quenching SV data will fall on a common line if one uses τ_0 as a scaling parameter. If differences persist, one will have to examine the possibility that there is a structural component to the mechanism of oxygen quenching, and this difference will then be reflected

(37) Geoffrey, G. L.; Wrighton, M. S. *Organometallic Photochemistry*, 1st Edition; Academic Press: New York, 1979.

(38) Rice, S. A. *Diffusion-Limited Reactions, Comprehensive Chemical Kinetics*; Bamford, C. H.; Tipper, C. R. H.; Compton, R. G., Eds.; Elsevier: Amsterdam, 1985; Vol. 25.

(39) Martinho, J. M. G.; Winnik, M. A. *J. Phys. Chem.* **1987**, *91*, 3640.

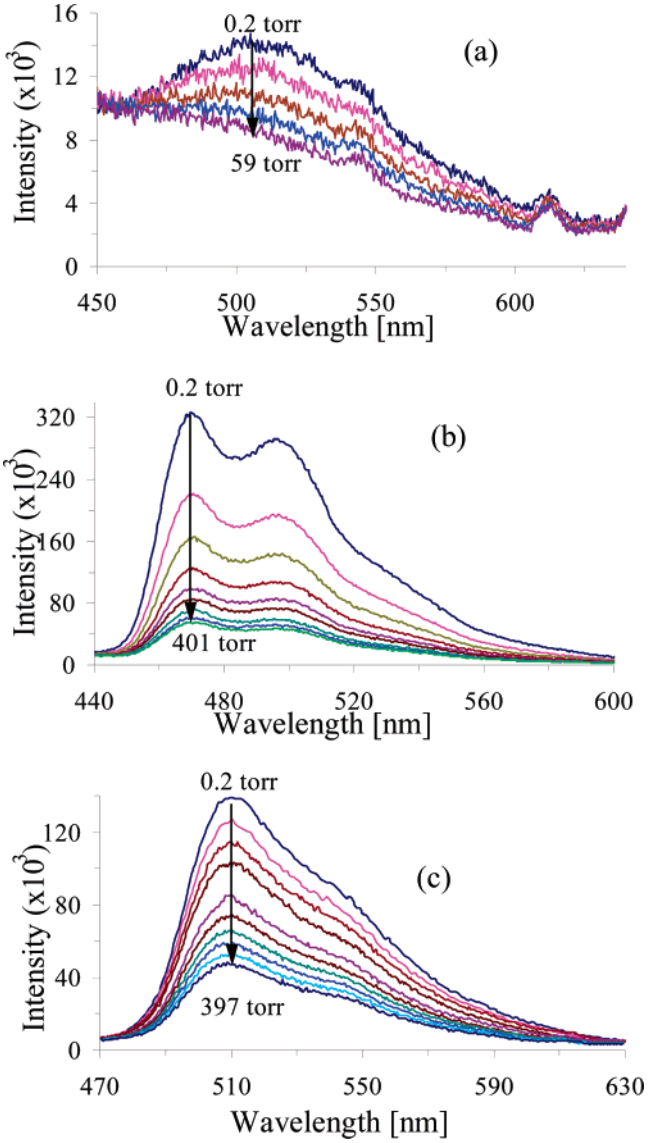

Figure 5. Oxygen quenching intensity spectrain *n*BuPTP at 25 °C of (a) sample **1A**, λ_{exc} = 340 nm, oxygen pressure range of 0.2−59 Torr and (b) sample **2A**, λ_{exc} = 340 nm, oxygen pressure range of 0.2−401 Torr, and (c) sample **3A**, λ_{exc} = 379 nm, oxygen pressure range of 0.2−397 Torr.

in different values of αR_{eff}. We will return to this point later in the paper.

2.4. Luminescence and Lifetime Studies. Steady-state luminescence experiments were conducted on samples in which the transition-metal complexes **1**, **2**, and **3** were dissolved in *n*BuPTP as a polymer film matrix. The films were exposed to air or pure oxygen with oxygen partial pressures in the range of p_{O_2} = 0.02−400 Torr. The data obtained at the lowest pressure were used to obtain I_0 and τ_0 values for subsequent data analysis. For each transition-metal complex, three film samples (**A**−**C**) were prepared with different dye loadings of 500 ppm (denoted by the suffix **A**), 1000 ppm (denoted by the suffix **B**), and 1500 ppm (denoted by the suffix **C**).

Steady-state PL spectra of samples **1A**, **2A**, and **3A** in the presence of different p_{O_2} values are shown in Figure 5. The data for samples **2A** and **3A** cover the full range of oxygen pressures, whereas that for sample **1A** are presented over a much more limited range of pressures (0.2−60 Torr). All of these samples have the same dye loading (500 ppm). Sample

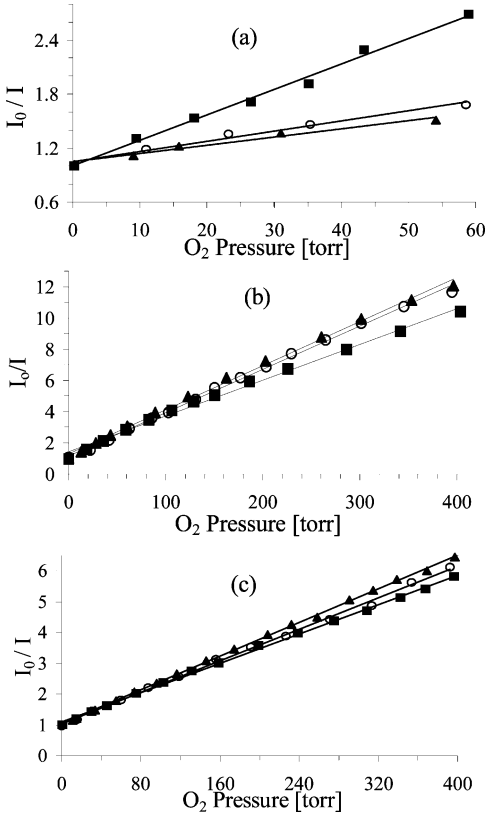

Figure 6. Oxygen quenching intensity data of (a) **1**, (b) **2**, and (c) **3** with dye loading of (▲) 500 ppm, (○) 1000 ppm, and (■) 1500 ppm.

1A shows a featureless emission spectrum with low emission intensity, relative to the emission spectra of samples **2A** and **3A**. Although the emission intensity of sample **1A** decreased as the oxygen concentration increased, as expected, repeated experiments on the same sample **1A** produced an emission spectrum with reduced intensity, which strongly suggests that complex **1** was degraded upon irradiation. In contrast, samples **2A** and **3A** show strong emission intensity. The luminescence is quenched by oxygen without distortions in the shape of the spectra. Experiments could be repeated on these samples, indicating a reasonable sample photostability.

SV plots of these emission intensities are presented in Figure 6, where we also compare samples **A**−**C** with different dye concentrations in the films. The important observation to be made in this figure is that the SV plots are linear. For dyes **2** and **3**, there is a very modest sensitivity of the SV slopes to dye concentration, whereas, for dye **1**, the effect is more pronounced. The K_{SV} values obtained from the slopes of these plots are listed in Table 2. Because of the photoinstability of dye **1**, we prefer not to try to interpret these results. The K_{SV} values for dye **2** are about twice as large as those for dye **3**. To develop a deeper understanding of the oxygen-quenching process, further experiments are needed. These experiments were performed only for dyes **2** and **3**, and only at the lowest dye concentration (500 ppm) in the polymer matrix.

In Figure 7, we present the PL decay curves of samples **2A** and **3A** obtained by pulsed-laser experiments for samples in the presence of an oxygen pressure of 0.20−400 Torr (air pressure up to 1950 Torr). All of these decay curves fit well to a single-exponential model.[16] From the samples at the

Table 2. Oxygen-Quenching Intensity Data at 298 K in the Pressure Range of 0−400 Torr of Oxygen (with Exceptions as Noted)

sample	excitation wavelength, λ_{exc} [nm]	dye loading [ppm]	$\lambda_{em,max}$ [nm]	K_{sv} [Torr^{-1}]	R^2	$I_0/I_{(159\ Torr)}$	intercept
			[Re(CO)$_3$(bpy)(CN-*t*-Bu)]Cl Dye				
1A	340, O_2 pressure of 0−60 Torr	500	507 (507[a])	0.0091	0.9702		1.05
1B	340, O_2 pressure of 0−60 Torr	1000		0.0114	0.9781		1.05
1C	340, O_2 pressure of 0−60 Torr	1500		0.0283	0.9927		1.00
			$Bu_4N[Ir(ppy)_2(CN)_2]$ Dye				
2A	340	500	470 (471[a])	0.0282	0.9967	6.04	1.31
2B	340	1000		0.0278	0.9973	5.87	1.14
2C	340	1500		0.0230	0.9936	5.37	1.42
			$Ir(ppy)_3$ Dye				
3A	370	500	510 (508[b])	0.0137	0.9994	3.36	1.05
3B	370	1000		0.0128	0.9982	3.20	1.09
3C	370	1500		0.0119	0.9985	3.02	1.09

[a] Measured in degassed CH_2Cl_2 solution. [b] Measured in degassed toluene solution.

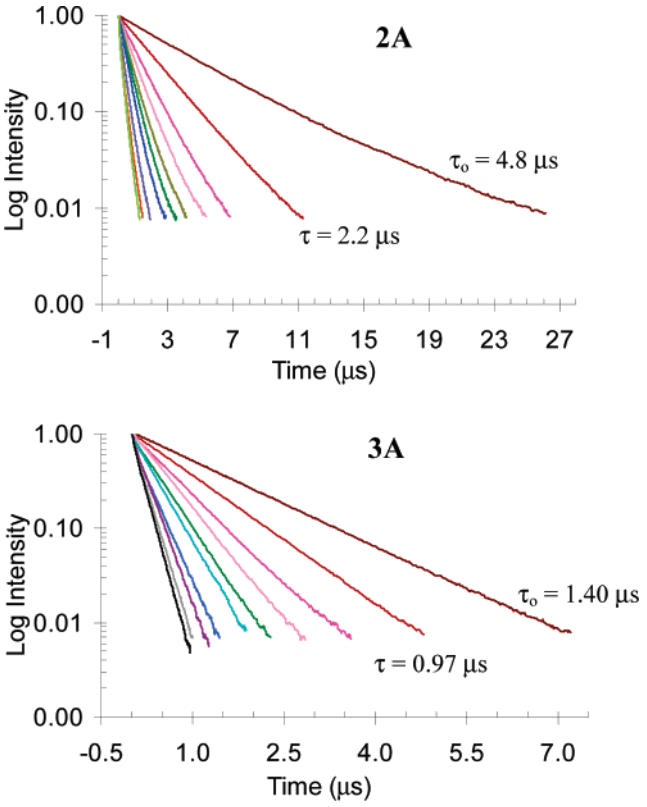

Figure 7. Decay spectrum from pulsed laser experiments of samples (a) **2A** and (b) **3A** in the pressure range of 0−260 kPa of air.

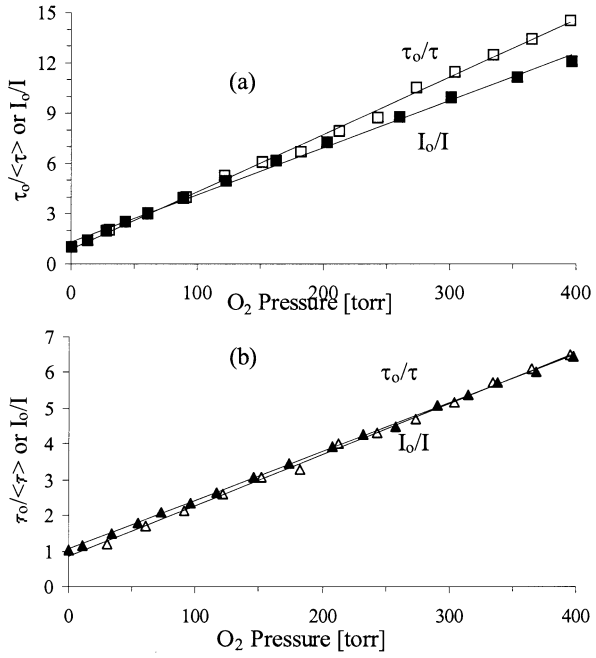

Figure 8. Stern−Volmer plots of data for (a) sample **2A** (from (□) luminescence and (■) lifetime quenching data) and (b) sample **3A** (from (△) luminescence and (▲) lifetime quenching data). Solid lines are the best-fit line using eq 1. Slopes are proportional to the product of oxygen permeability and the unquenched dye lifetime. (See Tables 1 and 2.)

Table 3. Air-Quenching Lifetime Data for Oxygen-Sensitive Films, 500 ppm Dye Loading[a] Lifetime Values Calculated by Fitting Luminescence Decay Profiles to a Single Exponential Decay

sample	excitation wavelength, λ_{exc} [nm]	lifetime, τ_0 [μs]	K_{sv} [Torr^{-1}]	k_q [10^9 M^{-1} s^{-1}]	R^2
2A	340	4.78 (3.22[b])	0.0343	5.5	0.9972
3A	379	1.40 (1.01[c])	0.0143	7.8	0.9989
PtOEP[d]		102	0.39	2.9	

[a] Lifetime values have been calculated by fitting luminescence decay profiles to a single exponential decay. [b] Lifetime measured in degassed CH_2Cl_2 solution. [c] Lifetime measured in degassed toluene solution. [d] Values taken from Lu et al.[21]

lowest air pressure, we obtained lifetimes of $\tau_0 = 4.78$ μs for sample **2A** and $\tau_0 = 1.40$ μs for sample **3A**. As expected, the excited-state lifetimes decreased as the oxygen concentration increased.

The SV plots from the intensity and lifetime measurements of samples **2A** and **3A** are shown in Figure 8. For both dyes, the plots of I_0/I and τ_0/τ exhibit a linear SV relationship. For sample **3A**, the lifetime SV plot is fully coincident with the intensity plot. For sample **2A**, there is a small difference in the slope (9%), which is difficult to explain. Lifetime K_{SV} values are presented in Table 3 and compared with values for PtOEP reported previously for the same polymer as a matrix. The important point is that the plots are linear, and the lifetime and intensity SV plots are almost identical. Thus, the dyes seem to be well-behaved in the *n*BuPTP matrix.

For effective oxygen-quenching dyes, a high oxygen-quenching rate constant k_q, as a consequence of a high SV constant K_{SV} with relative short lifetime, is also required. The quenching rate constant k_q can be calculated from the slope of SV plots and the known value of $S_{O_2} = 1.0 \times 10^{-3}$ M^{-1} atm^{-1} (eq 2), which was reported previously from the experiments of PtOEP in *n*BuPTP.[21]

In comparison to our previous studies of the SV behavior of complexes PtOEP ($k_q = 2.9 \times 10^9$ M^{-1} s^{-1}, $K_{SV} = 0.39$ Torr^{-1}), PtTFPP ($k_q = 2.0 \times 10^9$ M^{-1} s^{-1}, $K_{SV} = 0.17$

Table 4. Comparisons of Apparent P_{O_2} and αR_{eff} Values for Different Dyes in *n*BuPTP[a]

permeation parameter	$Bu_4N[Ir(ppy)_2(CN)_2]$	$Ir(ppy)_3$	PtOEP[b]	PtTFPP[b]	$[Ru(dpp)_3]Cl_2$[b]
P_{O_2} [10^{-12} mol s^{-1}]	7.5 (6.9)	10.7 (11.0)	4.0 (3.7)	2.6 (2.6)	2.0 (1.8)
αR_{eff} [nm]	1.88 (1.73)	2.67 (2.76)	1.0	0.65	0.5

[a] Values calculated from air-quenching lifetime data using 500-ppm-dye-loaded film samples. The data in parentheses are from intensity measurements. The apparent P_{O_2} values were obtained by fitting the SV slopes to eqs 6 or 7 assuming $\alpha R_{eff} = 1.0$ nm. [b] Values taken from Lu et al.[21]

$Torr^{-1}$), PtOEPK ($k_q = 2.6 \times 10^9$ M^{-1} s^{-1}, $K_{SV} = 0.22$ $Torr^{-1}$), and $[Ru(dpp)_3]Cl_2$ ($k_q = 1.6 \times 10^9$ M^{-1} s^{-1}, $K_{SV} = 0.013$ $Torr^{-1}$) immobilized in *n*BuPTP matrixes,[9,21] the oxygen-quenching rate constant of samples **2A** ($k_q = 5.5 \times 10^9$ M^{-1} s^{-1}, $K_{SV} = 0.0343$ $Torr^{-1}$) and **3A** ($k_q = 7.8 \times 10^9$ M^{-1} s^{-1}, $K_{SV} = 0.0143$ $Torr^{-1}$) were significantly higher. The k_q constants are almost double (sample **2A**) and triple (sample **3A**) the k_q value of PtOEP in *n*BuPTP. This indicates that samples **2A** and **3A** are very sensitive to oxygen quenching in *n*BuPTP.

2.5. Oxygen Permeability and the Effective Interaction Distance αR_{eff}. In a previous publication,[21] we described oxygen-quenching experiments for two platinum porphine derivatives (PtOEP, PtTFPP) and a ruthenium dye ($[Ru(dpp)_3]Cl_2$) dissolved in *n*BuPTP. For each individual dye, we found linear SV plots with essentially identical slopes for plots of I_0/I and τ_0/τ. The magnitudes of these slopes were different for each dye, and the variation could not be explained only in terms of a difference in unquenched lifetime τ_0. To interpret these experiments, we plotted the data according to eqs 6 and 7[21] (see Table 4). We then assumed a value of $\alpha R_{eff} = 1.0$ nm for PtOEP and calculated a value of $P_{O_2} = 4.0 \times 10^{-12}$ mol s^{-1} cm^{-1} atm^{-1} from the lifetime data and 3.9×10^{-12} mol s^{-1} cm^{-1} atm^{-1} from the steady-state intensity measurements.[21] Because P_{O_2} is a property of the polymer and not the dye, this value must be the same for each of the quenching experiments. Differences in the slopes of the plots according to eqs 6 and 7 were attributed to differences in sensitivity to quenching by oxygen. In this way, we determined that $\alpha R_{eff} = 0.5$ nm [$Ru(dpp)_3]Cl_2$, and 0.65 nm for PtTFPP, relative to the assumed value of 1.0 nm for PtOEP.[39]

Here, we extend this analysis to dyes **2** and **3**. To proceed, we replotted the data in Figure 8 according to eqs 6 and 7 (not shown) and calculated values of αR_{eff} from the slope using the value of $P_{O_2} = 4.0 \times 10^{-12}$ mol s^{-1} cm^{-1} atm^{-1} determined as previously described. In this way, we obtained $\alpha R_{eff} = 1.88$ nm for dye **2** calculated from the lifetime measurements and 1.73 nm from the intensity measurements. For dye **3**, we obtained $\alpha R_{eff} = 2.67$ nm (lifetime data) and 2.76 nm (intensity data).

These results lead to the rather surprising conclusion that photoexcited $Bu_4N[Ir(ppy)_2(CN)_2]$ (**2**) is ~1.8 times more sensitive to quenching per encounter with an O_2 molecule than PtOEP and 3.6 times more sensitive than $[Ru(dpp)_3]Cl_2$. The differences are even more pronounced for $Ir(ppy)_3$ (**3**), which is more than 2.5 times more sensitive to quenching by O_2 than PtOEP and more than 5 times more sensitive than $[Ru(dpp)_3]Cl_2$. These striking differences open interesting questions about the nature of the interaction between the quencher and the excited dye that lead to deactivation. Electron transfer or electron exchange must have an important role in the quenching process. There seem to be specific geometric requirements for quenching that vary from dye to dye. Within the platinum porphyrin series, we speculate that steric effects of the phenyl or pentafluorophenyl substituents of PtTFPP are likely responsible for the small reduction in quenching efficiency, compared to PtOEP with eight ethyl groups on the pyrrole rings but with the bridging carbons free of substituents. In the comparison of $Ir(ppy)_3$ with $[Ru(dpp)_3]Cl_2$, we speculate that steric effects may also be involved as a result of the present of bulky phenyl groups in the latter.

For the luminescent dyes to work well for PSP applications where the starting conditions are 1 atm of air, in addition to a high quantum yield of emission with relatively short excited lifetime, a value of $I_0/I_{(1\ atm)} \approx 2$ for 1 atm of air (159 Torr of oxygen) is also required. The $I_0/I_{(1\ atm)}$ ratio at an oxygen pressure of 159 Torr was not available with complex **1**, because, at pressures of >60 Torr, deviations from the linear SV plot exist for complex **1**. As shown in Table 2, the $I_0/I_{(1\ atm)}$ ratios at an oxygen pressure of 159 Torr of **2A**−**2C**) ($I_0/I_{(1\ atm)} = 6.0-3.6$) were well above the value of 2, whereas those values of **3A**−**3C**) ($I_0/I_{(1\ atm)} = 3.4-3.0$) were more similar to the value of 2 (see Table 2). This result indicates that, of all the dyes examined so far, complex **3** will be the most effective for PSP applications.

3. Conclusions

The iridium dyes $Bu_4N[Ir(ppy)_2(CN)_2]$ (**2**) and $Ir(ppy)_3$ (**3**) are characterized by high photoluminescence (PL) quantum yields and, for the dyes dissolved in *n*BuPTP polymer films, by excited-state lifetimes on the order of a few microseconds ($\tau_0 = 4.78$ μs for **2** and $\tau_0 = 1.40$ μs for **3**). Films that contain these dyes show a reduced PL intensity and more rapid excited-state decay rates in the presence of oxygen. The PL decay profiles remain exponential at all partial pressures of oxygen examined. Stern−Volmer (SV) plots were linear for both the intensity and lifetime data, with identical slopes for **3**. For **2**, the SV slope was ~9% steeper for the lifetime data than for the intensity data. When these data were interpreted quantitatively, we found values of $\alpha R_{eff} \approx 1.8$ nm for dye **2** and $\alpha R_{eff} \approx 2.7$ for dye **3**, compared to an assumed value of 1.0 nm for platinum octaethyl porphine (PtOEP). This means that, per encounter with an O_2 molecule, an excited dye **3** is 2.7 times more likely to be quenched than an excited PtOEP, and five times more likely to be quenched than the ruthenium dye $[Ru(dpp)_3]Cl_2$. Dye **2** is also more susceptible to quenching than PtOEP and $[Ru(dpp)_3]Cl_2$; however, the differences are not nearly as large.

For many oxygen sensor applications, one needs dye/matrix combinations in which the dyes are only partially quenched when the sensor is exposed to air at 1 atm ($p_{O_2} =$ 159 Torr), but which exhibit significant sensitivity to additional quenching, when exposed to higher air pressure.

One requirement is a high unquenched luminescence quantum efficiency, so that the sensor remains brightly luminescent, even when the emission is partially quenched. The high quantum yields of iridium dyes make them attractive for this type of application. For maximum sensitivity, intensity ratio (I_0/I) values in the presence of 1 atm air should be 2, indicating that half the excited states are quenched. Values of I_0/I for $p_{O_2} = 159$ Torr are listed in Table 2. These values are $I_0/I \approx 6$ for dye **2** and $I_0/I \approx 3.4$ for dye **3**. Thus, Ir(ppy)$_3$ in *n*BuPTP is a good, but not ideal, candidate for such applications.

Previous studies of PL oxygen sensors have identified the excited-state lifetime of the dye and the oxygen permeability of the polymer matrix as the two critical parameters in sensor design. We now see that a third factor that must be considered is the magnitude of αR_{eff} in the matrix (where α is the quenching efficiency per encounter and R_{eff} is the capture radius at which quenching occurs). If the magnitude of αR_{eff} for Ir(ppy)$_3$ in *n*BuPTP were identical to that of PtOEP, it would have the desired characteristic of an I_0/I value similar to 2.0 for 1 atm of air. Nevertheless, the value of $I_0/I = 3.4$ determined for this dye is close enough to warrant further experiments on this and other iridium dye derivatives.

Another characteristic of a useful sensor is that the dye can be incorporated at relatively high concentration without aggregation, spectral distortion, or self-quenching. This is particularly important when the time response of the sensor film is important, requiring the use of very thin polymer films. An effective way to increase the dye content in the film is to attach the dye to the polymer backbone covalently. This strategy has worked well for the cases of ruthenium dyes in *n*BuPTP.[10] Experiments to attach iridium dyes to *n*BuPTP are in progress, and the results will be reported in the future.

4. Experimental Section

4.1. Materials. The *tert*-butyllithium, tetrabutylammonium cyanide, 2-phenylpyridine, and 1,1,1-trichloroethane were used as received from Aldrich. Other solvents were dried according to standard methods. Hydrated iridium trichloride ($IrCl_3 \cdot xH_2O$) and rhenium carbonyl ($Re_2(CO)_{10}$) were purchased from Strem Chemicals and Pressure Chemicals Co., respectively. The [Bu_4N][Ir(ppy)$_2$(CN)$_2$] and fac-Ir(ppy)$_3$ complexes were synthesized according to literature procedure, and their purity was checked via nuclear magnetic resonance (^{1}H and ^{13}C NMR).[12,18,20] The *n*BuPTP was synthesized by following the reported procedure.[32,33,40]

Pyrex substrates were used to prepare films for luminescence measurements and pulsed-laser experiments. Dye-containing solutions were degassed using eight freeze−pump−thaw cycles on the standard all-glass vacuum line. Samples were then sealed under vacuum.

4.2. Analytical Measurements. Ultraviolet−visible (UV−vis) and infrared (IR) spectra were recorded in a 1-cm-path-length quartz cell on a Perkin−Elmer UV/VIS/NIR model Lambda 900 spectrometer and Fourier transform infrared (FT-IR) spectrometer, respectively. Emission spectra of solutions were recorded on an ISA Jobin Yvon-SPEX model FL3-22 fluorescence spectrometer. The emission lifetimes in solution were measured by exciting the pump−freeze−thaw sample operated in nanosecond time-correlated single-photon counting mode. Photoluminescence spectra of film samples were measured at various oxygen concentrations using a Spex Fluorolog spectrometer. Lifetime decay of dye-containing films were measured using Nd:YAG laser (Spectra Physics GRC 170). Signals were detected with a simple photomultiplier tube and digitized by a Tektronix Programmable Digitizer 7912AD. A high-power attenuator (model 935-10, Newport) controlled the light intensity that was exciting the sample. The ^{1}H and ^{13}C NMR spectra were measured with a Varian Gemini 300 spectrometer at 300 MHz and a Varian Unity 400 spectrometer at 400 MHz, respectively. The reported chemical shifts are reported relative to trimethylsilane (TMS).

*4.2.1. Synthesis of [Re(CO)$_3$(bpy)(CN-t-Bu)]Cl (**1**).* Chloride ligand exchange of Re(CO)$_3$(bpy)Cl,[41−43] with an equimolar amount of $AgOSO_2CF_3$, gave a rhenium(I) triflate species.[22] A mixture of Re(OTf)(CO)$_3$(bpy) (277 mg, 0.481 mmol) and Na[BAr′$_4$] (426 mg, 0.481 mmol) was stirred for 30 min in CH_2Cl_2 (86 mL) followed by the addition of CN-*t*-Bu (55.0 μL, 0.482 mmol). The resulting solution was stirred for 2 days and filtered to remove sodium triflate. The filtrate was reduced to ca. 8 mL, and the diffusion of dry hexanes over 2 days yielded a yellow crystalline solid product, 556 mg (69%).

^{1}H NMR: (400 MHz, CD_2Cl_2) 9.0 (dd, $J = 4.79$ Hz, 2H bpy), 8.26 (d, $J = 7.98$ Hz, 2H bpy), 8.18 (dt, $J = 7.98$ Hz, 2H bpy), 7.72 (d, $J = 2.39$ Hz, 8H H−C_{ortho} BAr′4), 7.6 (dt, $J = 5.59$ Hz, 2H bpy), 7.55 (s, 4H H−C_p BAr′$_4$), 1.25 (s, 9H, CH_3). ^{13}C NMR: (400 MHz, CD_2Cl_2) 191.8 (2CO), 188.0 (CO), 162.4 (q, C_iBAr′$_4$) 156.2 (bpy), 154.4 (bpy), 141.1 (bpy), 135.4 (C_{ortho}BAr′$_4$), 129.5 (m, C_mBAr′$_4$), 123.0, 124.49 (bpy), 118.1 (q, C_pBAr′$_4$), 59.9 ($(CH_3)_3C$), 30.3 ($(CH_3)_3C$).

Counterion exchange of [Re(CO)$_3$(bpy)(CN-*t*-Bu)]BAr′$_4$ to [Re(CO)$_3$(bpy)(CN-*t*-Bu)]Cl was performed in a saturated acetone solution of tetrabutylammonium chloride. The exchange was confirmed by the disappearance of BAr′$_4$ anion peaks in the ^{1}H NMR spectrum.

*4.2.2. Single-Crystal X-ray Structural Determination of **1**.* Data were collected on a Nonius Kappa-CCD diffractometer using monochromated Mo Kα radiation and were measured using a combination of ϕ scans and ω scans with κ offsets, to fill the Ewald sphere. The data were processed using the Denzo-SMN package.[44] Absorption corrections were performed using SORTAV.[45] The structure was solved and refined using SHELXTL V6.1[46] for full-matrix least-squares refinement that was based on F^2. All H atoms were included in calculated positions and allowed to refine in riding-motion approximation with U∼iso∼ tied to the carrier atom. Crystallographic data for the compound is given in Table 1.

4.2.3. Preparation of the Dye-Containing nBuPTP Film. The *n*BuPTP was dissolved in 1,1,1-trichloroethane to give a 50 mg/mL solution. Dyes **1** and **3** were dissolved CH_2Cl_2 and dye **2** was dissolved in toluene. An appropriate amount of dyes solution were added to the polymer solution to achieve a dye loading of 500, 1000, and 1500 ppm. Three drops of the dye-containing polymer solution were deposited on a microscope slide and allowed to dry in darkness while exposed to the open air for 24 h. The films were

(40) Suzuki, D.; Akagi, H.; Matsumura, K. *Synth. Commun.* **1983**, 369.
(41) Schmidt, S. P.; Trogler, W. C.; Basolo, F. *Inorg. Synth.* **1991**, *28*, 161.
(42) Caspar, J. V.; Meyer, T. J. *J. Phys. Chem.* **1983**, *87*, 952.
(43) Wrighton, M.; Morse, D. L. *J. Am. Chem. Soc.* **1974**, *96*, 998.
(44) Otwinowski, Z.; Minor, W. *Methods Enzymol.* **1997**, *276*, 307.
(45) Blessing, R. H *Acta Cryst.* **1995**, *A51*, 33.
(46) Sheldrick, G. M. SHELXTL/PC. Version 6.12 Windows NT Version, Bruker AXS Inc., Madison, WI, 2001.

subsequently heated in a vacuum oven (ca. 1 Torr) at 60 °C for 48 h. The final films were typically 30−50 μm thick.

4.2.4. Photoluminescence Measurements. Films on their substrates were loaded into a gas pressure/vacuum cell in the sample chamber of the fluorescence spectrometer and subjected to vacuum for 24 h to measure the unquenched PL spectra of the film at zero oxygen concentration. A preset amount of air or oxygen was introduced into the pressure/vacuum cell. PL spectra or lifetimes of the film were obtained after a wait of at least 3 min, to allow the sample to equilibrate with the surrounding atmosphere. Control experiments indicated that this time was sufficient for measured intensities to remain stable. Air or oxygen pressure inside the cell was controlled over a range of 0−1000 Torr, through a combination of a vacuum pump and a compressed gas line. Gas pressure was measured by a MKS Baratron 626A 13TAE absolute pressure transducer (with an accuracy of ±0.15% in the range of 10−1000 Torr).

Acknowledgment. The authors thank NSERC Canada for a strategic grant and the Royal Canadian Mounted Police (RCMP) for their support of this research. I.M. also thanks the Canadian Government for a Canada Research Chair.

Supporting Information Available: CIF data regarding Re complex **1**. This material is available free of charge via the Internet at http://pubs.acs.org.

CM047794R